ORGANIC PROCESS RESEARCH & DEVELOPMENT
OPR&D

pubs.acs.org/OPRD

Article

High-Throughput Crystallization Screening Technique with Transmission PXRD Analysis

Victor W. Rosso,* Zhiwei Yin, Heba Abourahma, Ariel Furman, Shasad Sharif, Andrew Werneth, Jason M. Stevens, Frederick Roberts, Darpandeep Aulakh, Roger Sommer, and Amy A. Sarjeant

Cite This: *Org. Process Res. Dev.* 2023, 27, 1437−1444

Read Online

ACCESS | Metrics & More | Article Recommendations | Supporting Information

ABSTRACT: The ability to quickly generate and identify crystalline solids for organic compounds in a parallel fashion requires a rapid, adaptable crystallization screening strategy that delivers reliable, valuable, and consistent results. The key to the system is a standard platform small-scale (0.5−2 mg) crystallizer screening array that reproducibly crystallizes compounds and facilitates the presentation of crystallization samples to both an automated polarized light microscope and an instrument capable of PXRD analysis. Data science technologies were leveraged to streamline the workflow of data visualization and processing. The fully developed workflow successfully used both single-crystal and PXRD analyses to identify multiple polymorphs of a test compound in a single screening experiment on 200 mg of input material with commercially available crystallizers and instruments to perform a highly detailed crystallization screening study. The methods and techniques described herein are fully transferrable to those working in the synthetic organic chemistry field.

KEYWORDS: *crystallization, screening, polymorph, PXRD*

INTRODUCTION

For a small-molecule drug development organization, the ability to rapidly generate and identify crystalline materials for active pharmaceutical ingredients (APIs) and synthetic intermediates is a key capability to ensure that processes afford developable solid-state forms that produce high-quality drug candidates and intermediates.[1,2] Over the past two decades, high-throughput crystallization systems have evolved, supported by the development of both laboratory automation solutions in conjunction with ancillary software development to enable recording, storage, analysis, and reporting of parallel crystallization results.[3] These efforts began as simple sets of tools such as a glass 96-well plate and a microscope that with time evolved toward more sophisticated workflows, which integrated hardware tools such as parallel crystallization vessels with analytical instruments and supporting software. Currently, high-throughput crystallization is routinely used to support internal pharmaceutical development efforts.[4]

A common attribute of high-throughput crystallization techniques is the ability to efficiently analyze crystalline samples by several techniques. Previously published approaches performed small-scale crystallizations in conical vessels linked to both image and predominantly in situ Raman analysis.[5−8] Another iteration involves multiple crystallization techniques in customized 96-well plates that upon disassembly allows samples to be analyzed by microscopy, Raman, and reflectance PXRD.[9] An earlier internal version primarily used light microscopy and LC quantitation to assess mg-scale well plate experiments.[10,11]

As projects progressed through high-throughput crystallization, and were further developed, the interpretation of forms predominantly transitions to PXRD analysis. PXRD collection has been reported at a high-throughput crystallization scale, albeit with some challenges associated with a preferred orientation.[5] Therefore, the ability to directly collect PXRD data, preferably in transmission mode, while minimizing preferred orientation, was pursued. Additionally, crystallization arrays that were able to generate samples of sufficient size for single-crystal X-ray diffractometer analysis afforded even more advantages. When appropriate-sized crystals are generated, the confirmation of the physical and chemical forms of each hit of the early-stage project provides tremendous insight and direction when selecting conditions to scale up by directing us toward more desirable materials (neat forms > hydrates > solvates). Continued development of the workflow, illustrated in Figure 1, now includes both the addition of single-crystal and PXRD analyses to supplement capabilities associated with prior techniques.

To test the high-throughput crystallization workflow, replicate trial studies of compound **1** (Figure 2), 5-methyl-2-[(2-nitrophenyl)amino]-3-thiophenecarbonitrile (ROY),[12,13] were undertaken. ROY is well known to be highly polymorphic and therefore is an excellent candidate to probe the capability limits of the parallel crystallization equipment. ROY was treated in the same manner as an API with unknown solubility. The first goal was to assess the reproducibility of crystallization results given that multiple upgrades had occurred to the crystallizers. Understanding how small-scale operations coupled with the

Received: March 20, 2023
Published: June 20, 2023

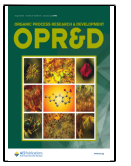

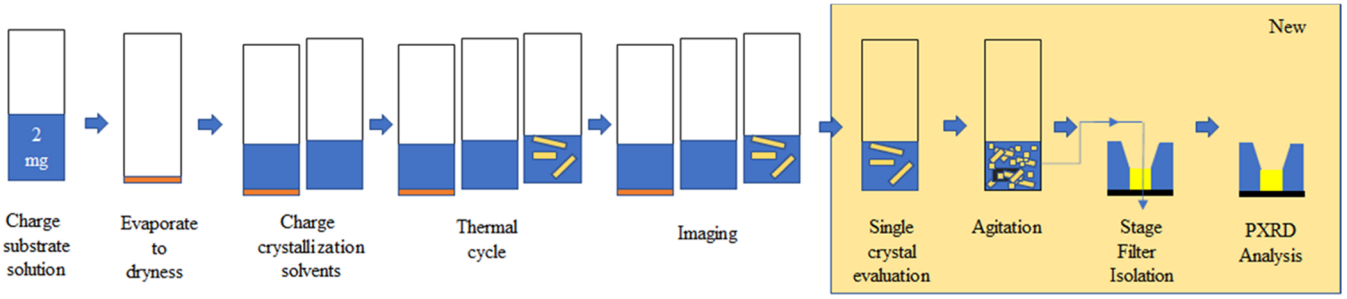

Figure 1. Illustration of the steps associated with an integrated high-throughput crystallization workflow.

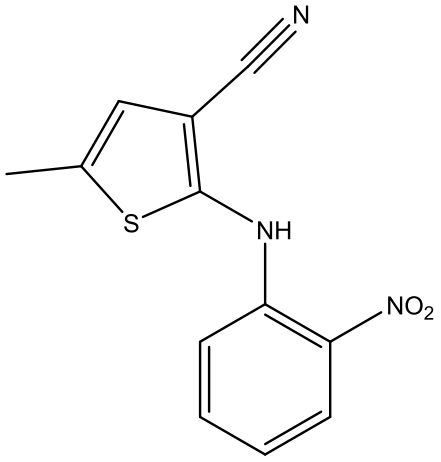

1

Chemical Formula: $C_{12}H_9N_3O_2S$
Molecular Weight: 259.28

Figure 2. Model compound, 5-methyl-2-[(2-nitrophenyl)amino]-3-thiophenecarbonitrile (ROY) for the crystallization study.

variability of nucleation event occurrence is critical in the interpretation of the results of an automated crystallization study. These samples also provided sufficiently large crystals to demonstrate that single-crystal XRD data could be collected from 96-well plate samples. Finally, a parallel PXRD capability with various scales of input material from 0.5 to 4 mg was demonstrated. This allowed the assessment of crystallinity of various samples and was applied to a standard screening array to successfully detect multiple polymorphs in a single 96-well plate.

METHODS

Substrates for this study are charged to the crystallizers as stock solutions in volatile solvents and evaporated to dryness. A stock solution (1) was prepared by dissolving 200 mg of ROY (TCI Chemicals, >97% purity, OP form with extra peaks present) in 5 mL of MeCN (40 mg/mL), and 50 μL (2 mg) of the ROY stock solution was manually charged to an array of 96 vials (8 × 30 mm vials) residing in a Photoredox block with a multichannel pipettor. The samples were evaporated to dryness in an evaporative centrifuge whereupon red or orange and occasionally yellow solids are observed in the wells. A manual addition of a total volume of 100 μL of crystallization solvent(s) was charged to the vials with a multichannel pipette. In cases where

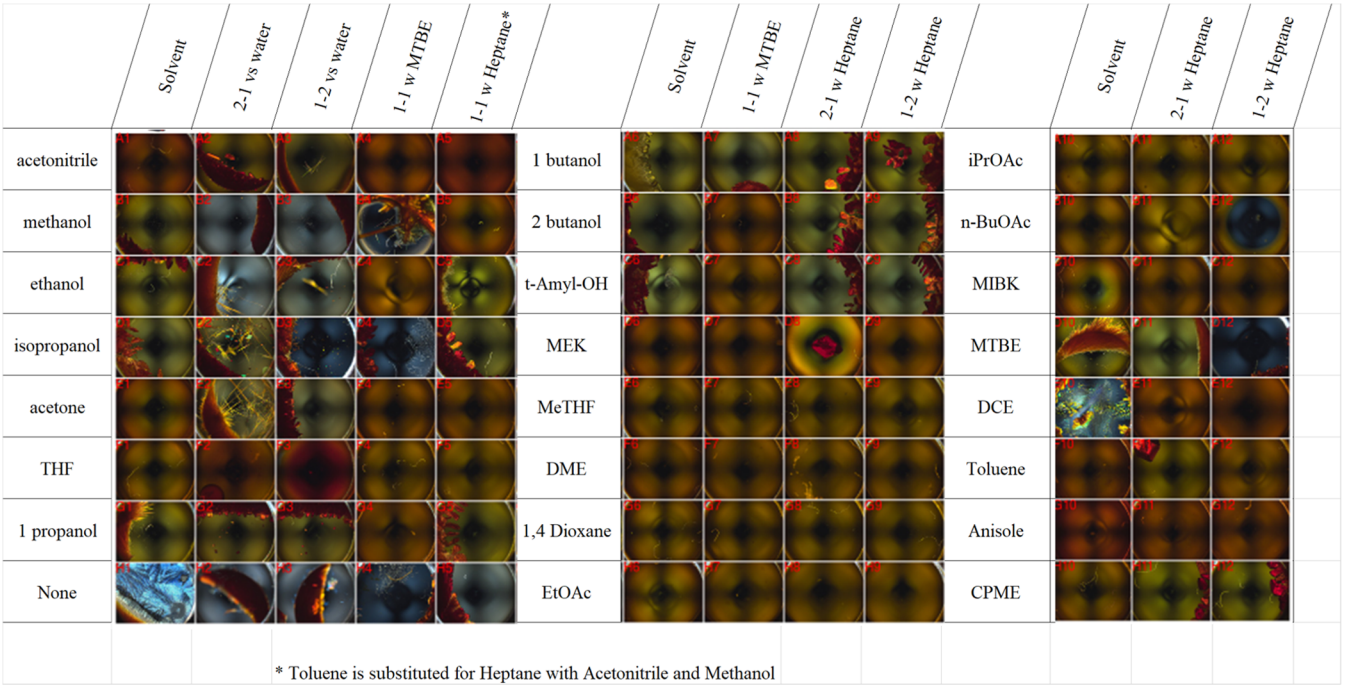

Figure 3. Images collected from the standard screening array loaded with 2 mg of ROY per well.

https://doi.org/10.1021/acs.oprd.3c00091
Org. Process Res. Dev. 2023, 27, 1437−1444

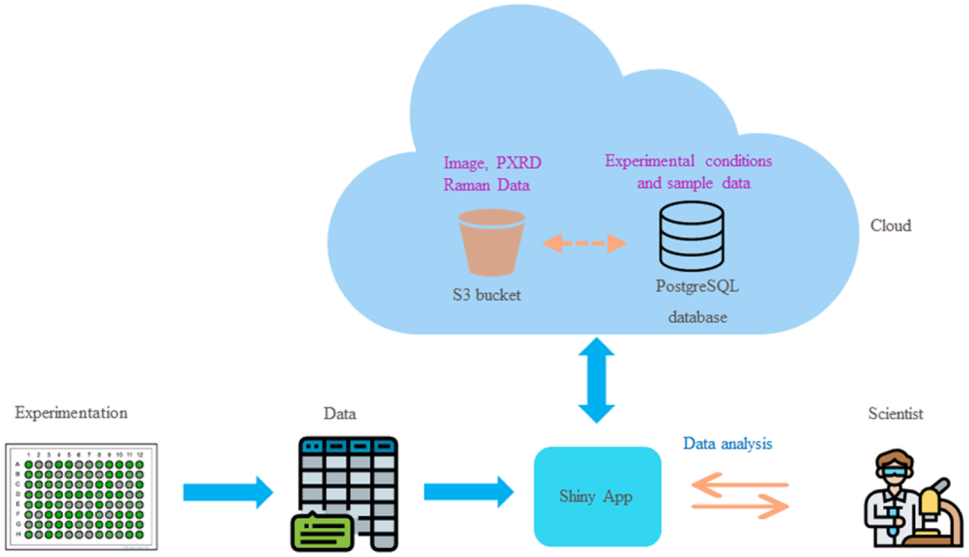

Figure 4. Overview of data collection, storage, analysis, and reporting for high-throughput crystallization.

multiple solvents are present, the mixtures were prepared in situ with water and heptane charged last. An overview of the solvent array, which is generally used to screen new compounds is shown in Figure 3 and shared in Supporting Materials. The samples were then subjected to a thermal cycling treatment (50 °C for 2 h followed by a 6 h linear cooling ramp to 20 °C, repeated 6×) and aging process (>12 h ambient temperature in a model IN30 Torrey Pines Scientific EchoTherm chilling incubator).

After thermal cycling and aging, microscope images were collected with a Zeiss Axio Observer.Z1m Polarized Light Microscopy (PLM) instrument, which included a plate reader stage, 2.5× objective, an AxioCam MR R3, and Zen 2 software. Images were stored on a common lab drive.

Software shown in Figure 4 is then used to archive the data. Sets of raw images and spreadsheets of solvent systems are assembled in the R Shiny App, which is an open-source web application framework for R programming language that allows you to build interactive web applications directly from R scripts. This is where users upload and download data, analyze the data, and produce reports. The combined data set (images, experimental details) is then uploaded to the cloud. The images are loaded to an S3 bucket (a container for storing objects), a cloud storage service that allows you to store and retrieve data from anywhere on the web. A data table describing the chemical contents of each well and the metadata (such as ELN, thermal profile, project information, crystallization type stored as Java Script Object Notation (JSON) strings) is stored in PostgreSQL database, an open-source relational database management system that is used to store and manage data. All of this is coordinated by an Amazon Relational Database Service (RDS), which is a web service provided by Amazon Web Services (AWS) that makes it easy to set up, operate, and scale a relational database in the cloud.

The resulting crystals were then evaluated by a crystallographer. We focused on crystals of sufficient size for our diffractometer (between 0.1 and 0.5 mm average dimensions), which had well-defined faces and extinguished plane-polarized light when rotated through it and showed no evidence of twinning or splitting. As the different polymorphs of ROY are well characterized previously, we chose 3 representative forms for single-crystal structure determination to demonstrate the capability of this technique to generate suitable crystals for single-crystal analysis. Crystals that appeared suitable for single-crystal analysis as per the criteria described above were manually retrieved from their respective wells by a small dissecting probe coated with a small amount of Paratone-N oil, a common cryoprotectant used for single-crystal experiments. These crystals were then visually analyzed under a polarized light microscope to isolate one of suitable size and shape. The crystal used for analysis was then scooped from the Paratone-n oil onto a MiTeGEN loop and placed on the diffractometer for data collection and subsequent structure determination. Red was obtained directly from a well containing 2-BuOH/heptane. Orange was obtained from iPrOAc/heptane in well that crystallized after sample transfer to the single-crystal laboratory. Yellow was obtained from a well containing CPME/heptane that utilized a paper wick to remove the solvent from the crystallizer.

After this crystallographic evaluation, magnetic stir bars were then charged to the plate followed by tumble agitation at 500 rpm for 1 h, prior to a manual transfer of the slurry onto a PXRD stage filter[14] with a 12-channel pipette. The PXRD stage filter was then mounted on a Bruker D8 discovery PXRD system configured in transmission mode. Each sample was analyzed for 60 s to afford PXRD patterns in the range of 3−35 2θ.

To evaluate the ability to collect PXRD data, a custom design was performed such that each row contained a loading of 0.5, 1, 2, or 4 mg of ROY with crystallization solvents of either 1:2 isopropyl alcohol/water or 1:2 *tert*-amyl alcohol/heptane. Microscopic images were collected, and then the entire plate was harvested for PXRD analysis using the methods described above.

RESULTS AND DISCUSSION

The core capability is to screen for crystals of various substrates with unknown solubility properties. The solvent combination array illustrated in Figure 3 consists of commonly used solvent pairs covering a broad swath of crystallization space of varying polarities and solubilizing properties from pure heptane to pure water and many points in between. This design is applied broadly to most compounds as they arrive with limited solubility information. The solvent array is referred to as a 5-4-3 array with

https://doi.org/10.1021/acs.oprd.3c00091
Org. Process Res. Dev. 2023, 27, 1437−1444

	Solvent	2-1 vs water	1-2 vs water	1-1 w MTBE	1-1 w Heptane*		Solvent	1-1 w MTBE	2-1 w Heptane	1-2 w Heptane		Solvent	2-1 w Heptane	1-2 w Heptane
Acetonitrile	0	3	6	1	0	1 butanol	6	1	6	6	iPrOAc	0	1	3
Methanol	5	5	3	1	0	2 butanol	6	0	6	6	n-BuOAc	0	0	3
Ethanol	6	6	5	1	6	t-Amyl-OH	6	1	6	6	MIBK	0	0	0
Isopropanol	6	6	6	2	6	MEK	0	0	1	1	MTBE	4	6	6
Acetone	0	5	4	2	1	MeTHF	1	0	0	2	DCE	1	0	0
THF	0	1	1	0	0	DME	0	0	0	0	Toluene	0	3	3
1 Propanol	5	6	6	2	6	1,4 Dioxane	0	0	0	0	Anisole	0	0	0
None	6	6	6	6	6	EtOAc	0	0	0	0	CPME	0	3	5

Figure 5. Scoring of the number of wells with observable crystals by polarized light microscopy (n = 6) from six replicate studies.

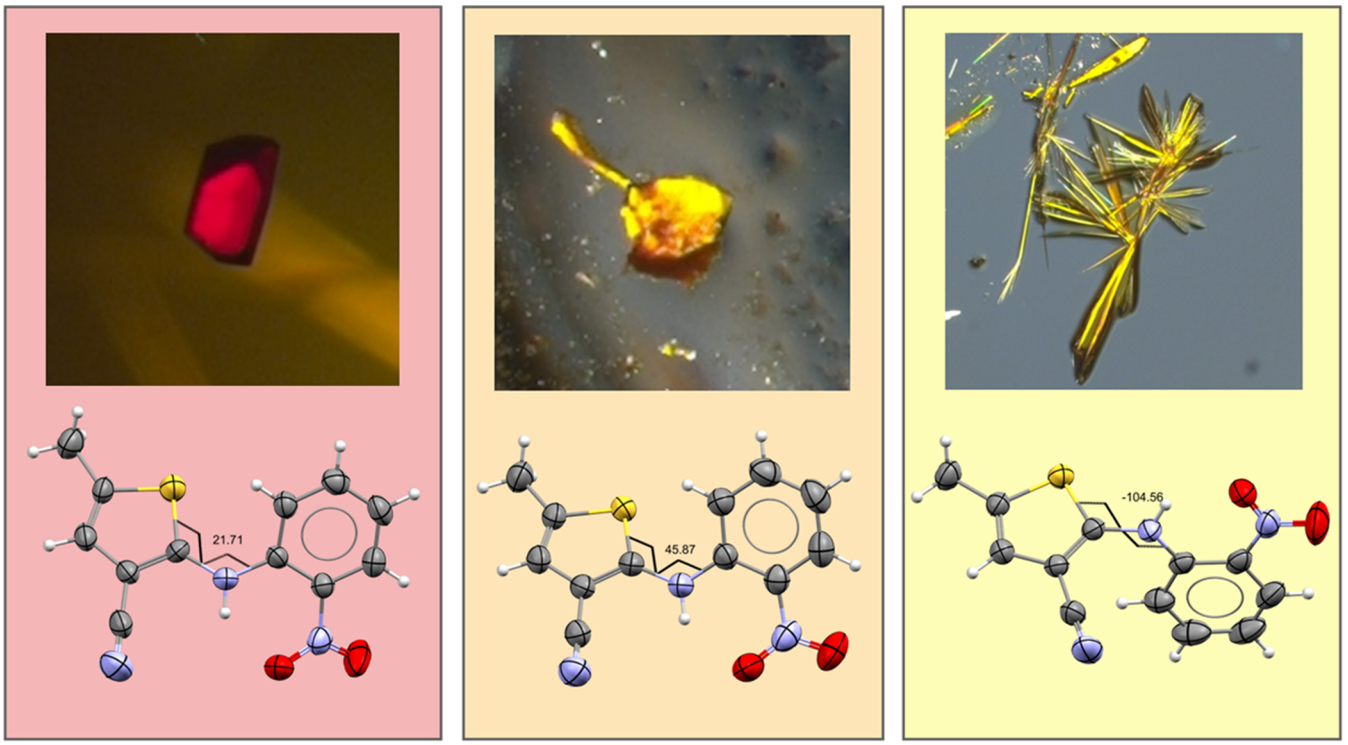

Figure 6. Three crystal structures determined as part of this study: Red (top), orange (middle), and yellow (bottom) showing their different unit cell determinations and the distinguishing torsion angle dimensions for each polymorph.

the left-hand 5 columns of the plate containing water-miscible solvents such as acetone, which is miscible with both water and nonpolar solvents such as heptane. The middle 4 columns and right-hand 3 columns of the plate contain water-immiscible solvents of decreasing polarity and are used in combination with MTBE and/or heptane. The layout of this array of solvents in the plate was designed to be readily dispensed with the use of a multichannel pipettor.

The initial dissolution of the substrate in a volatile organic solvent (such as acetonitrile or dichloromethane) provides key insight into the solubility of the molecule for the purposes of adjusting the design of the array. If the compound can be dissolved and dispensed in a low boiling organic solvent, the standard 5-4-3 array will be used. Should the substrate instantaneously dissolve in the first drops of solvent, the array can be adjusted by increasing the water, heptane, and MTBE content in the columns. Should the substrate be difficult to dissolve in a low boiling solvent, then the array can be modified by substituting more polar solvents such as DMA, NMP, or DMF for water, heptane, and MTBE. Iterations of this standard array have been successfully used to study hundreds of molecules.

The small-scale crystallizer platform or the plate itself is equally important as the solvent array. We utilized a commercially available standard 96-position photoredox plate,[15] which has a standard 8*30 mm shell vial, as the crystallizer and a Zeiss automated microscope modified by the vendor to visualize the wells of the photoredox plate within the focal plane of the microscope. Key features of the crystallizer include a removable sealing septum that can be incubated to 50 °C while minimizing solvent loss during thermal cycling, and the open bottom combined with a removable top allows us to directly collect PLM images without the need to manipulate the samples further.

The goal of this study was to assess and understand the reproducibility of crystallization in small-scale studies routinely performed with this equipment. Figure 3 illustrates images acquired from a typical screen performed on the test compound ROY, utilizing the standard 5-4-3 array of solvent combinations. Crystallization can be readily observed in about 40% of the wells

https://doi.org/10.1021/acs.oprd.3c00091
Org. Process Res. Dev. 2023, 27, 1437−1444

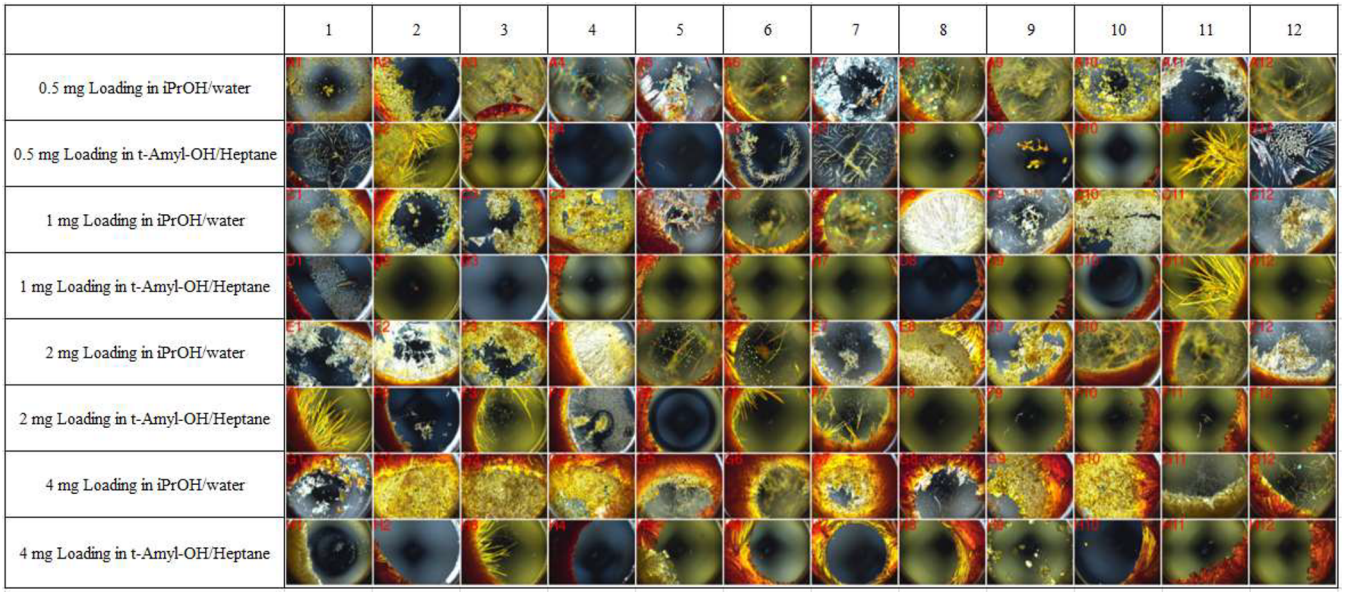

Figure 7. Images from the ROY test plate to collect PXRD data as a function of loading and crystallization solvent.

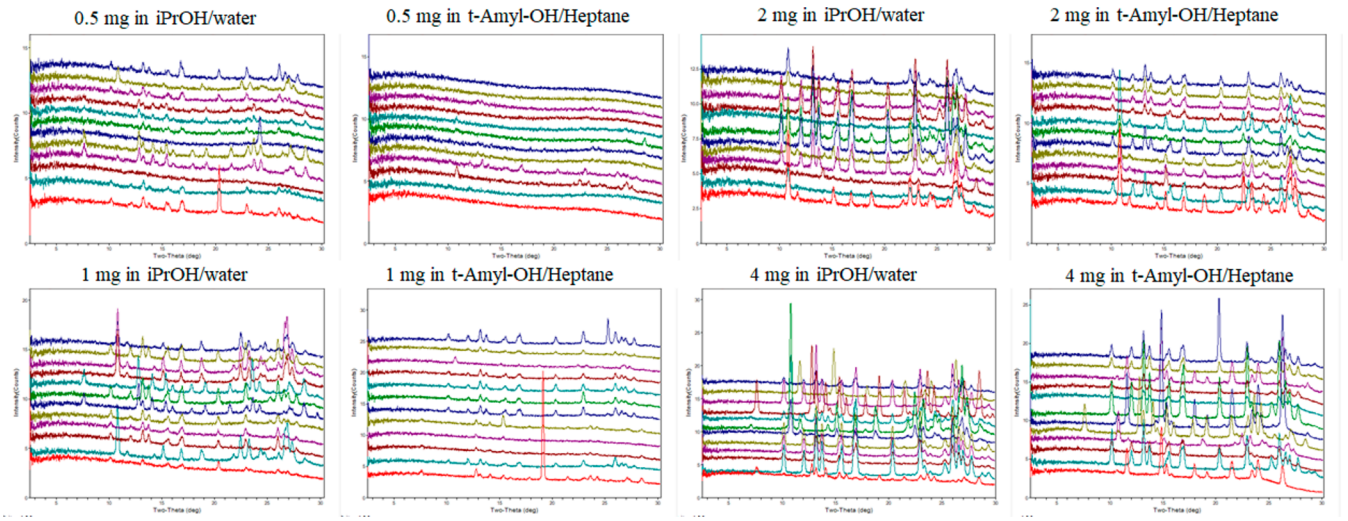

Figure 8. Collection of PXRD data (60 second acquisition time) from each well by varying the loading and solvent system.

that were loaded with 2 mg of ROY and is considered successful if birefringent crystals are observed by PLM in a well.

The data generated with replicates of a known compound provide an understanding of the variability associated with crystallization processes on a small scale. In our hands, when comparing two plates utilizing the same crystallization array with a compound that crystallizes in about half the wells, generally about 15% of the wells afforded different results (as defined by whether crystals were observed by PLM). This correlation rate is near levels achieved in previous iterations of our system that utilized glass 96-well plates where the optimization of reproducibility from as low as 50% was driven primarily by the ability to prevent solvent evaporation. This level of reproducibility establishes confidence that the crystallizers are functioning properly. Factors that influence the reproducibility of crystallization outcomes include variability introduced with minor amounts of solvent evaporation as well as the reliance upon nucleation occurring with minimal amounts of material.

To probe reproducibility, a series of 6 replicate plates of ROY were performed independently by 4 different scientists. The experimental outcome is illustrated in Figure 5 where the number represents the number of times from 0 to 6; birefringent crystals were observed in each well of the 5-4-3 solvent array. In this study, 50 of the wells had low success rates (37 = 0, 13 = 1) and 33 wells were consistently successful, producing crystals in ⩾5 plates (6 = 5, 27 = 6).

A total of 13 wells (14% of the plate) afforded variable results, which may represent regions that are more susceptible to both solvent retention and small perturbations that may affect the occurrence of nucleation events. Overall, >85% of the experimental array provided reasonably consistent results given the variability associated with this type of experimentation and among different scientists who performed the studies.

Crystallography: Figure 6 illustrates 3 structures that were obtained directly from high-throughput crystallization plates for ROY. There are 62 structure determinations of the various polymorphs in the CSD (v. 5.43 with all updates); of those, 35 include atomic coordinates from the refinement. The average *R*-factor for these 35 structures is 3.94% with a range between 0.94 and 10.48%. The *R*-values of the structures reported here are

https://doi.org/10.1021/acs.oprd.3c00091
Org. Process Res. Dev. 2023, 27, 1437−1444

														Crystallinity score	
mg Loading	Solvent	1	2	3	4	5	6	7	8	9	10	11	12	Total <3.2	Total > 3.2
0.5	iPrOH/water	4.7	2.9	3.8	4.3	3.2	3.2	3.2	3.3	3.5	3.5	3.6	4.0	2	10
0.5	t-Amyl-OH/heptane	3.0	3.3	3.1	2.9	2.9	3.0	3.0	2.9	3.0	3.1	3.0	3.0	11	1
1	iPrOH/water	3.4	4.1	3.5	3.9	4.7	5.3	5.6	5.4	7.4	5.5	6.7	5.0	0	12
1	t-Amyl-OH/heptane	3.2	3.0	3.6	4.1	4.0	4.3	3.9	3.7	6.4	3.4	3.4	6.6	2	10
2	iPrOH/water	6.7	4.4	6.4	6.0	10.8	10.6	3.4	9.9	7.5	3.9	3.6	4.5	0	12
2	t-Amyl-OH/heptane	8.0	4.2	4.9	4.9	5.4	3.9	6.4	3.9	4.3	5.8	4.4	4.7	0	12
4	iPrOH/water	4.8	7.9	10.9	12.7	6.7	15.9	12.6	18.2	14.2	17.8	9.1	5.7	0	12
4	t-Amyl-OH/heptane	7.4	6.5	5.4	11.9	16.1	18.5	4.4	5.4	8.9	10.8	6.5	8.6	0	12

Figure 9. Calculated crystallinity scores of PXRD samples from the loading study.

mg Loading	Solvent	1	2	3	4	5	6	7	8	9	10	11	12
0.5	iPrOH/water	OP	a/wc	R	R	a/wc	OP	R	OP	R	OP	ON	OP
0.5	t-Amyl-OH/heptane	a/wc	ON	OP	a/wc	a/wc	a/wc	a/wc	a/wc	a/wc	a/wc	a/wc	a/wc
1	iPrOH/water	OP	OP	OP	OP	R	OP	R	ON	ON	OP	ON	ON
1	t-Amyl-OH/heptane	a/wc	a/wc	R	OP	OP	OP	OP	OP	wc/R like	OP	ON	OP
2	iPrOH/water	ON	ON	OP	ON	OP	OP	ON	OP	OP	ON	ON	ON
2	t-Amyl-OH/heptane	ON	ON	ON	ON	OP	ON	ON	OP	OP	OP	OP	OP
4	iPrOH/water	R	OP	OP	OP	ON	ON	ON+1 pk	R	OP	OP	Y	OP
4	t-Amyl-OH/heptane	Y	OP	ON	R	Y	OP	OP	OP	Y	OP	OP	OP

Figure 10. Assignment of forms of PXRD samples from the loading study (forms observed = R, OP, ON, Y).

	Solvent	2-1 vs water	1-2 vs water	1-1 w MTBE	1-1 w Heptane*		Solvent	1-1 w MTBE	2-1 w Heptane	1-2 w Heptane		Solvent	2-1 w Heptane	1-2 w Heptane
acetonitrile		OP (7.90)	Y (5.67)	ON (4.52)		**1 butanol**	ON (7.47)		ON (6.45)	ON (3.97)	**iPrOAc**		Amorph (2.84)	ON (4.31)
methanol	OP (5.80)	ON (4.89)	ON (7.93)			**2 butanol**	ON (8.35)		ON (7.33)	ON (6.17)	**n-BuOAc**			ON (6.58)
ethanol	ON (8.08)	ON (8.82)		ON (6.70)	ON (10.5)	**t-Amyl-OH**		ON wk (3.61)	ON (4.64)		**MIBK**			ON wk (3.76)
isopropanol	ON (4.58)	ON (8.08)	ON (5.45)	ON (4.97)		**MEK**			ON wk (3.32)	ON (4.45)	**MTBE**	ON (4.71)	OP (6.98)	
acetone	Amorph (2.78)	Y (5.55)	Amorph (2.84)	Amorph (3.01)		**MeTHF**					**DCE**			
THF		Y (4.56)				**DME**					**Toluene**		ON wk (3.33)	ON (4.97)
1 propanol	ON (3.61)	ON (9.75)	ON wk (3.43)	ON wk (3.82)		**1,4 Dioxane**					**Anisole**			Amorph (2.86)
None	ON (9.93)	ON wk (3.56)	ON wk (3.45)	Amorph (3.09)		**EtOAc**					**CPME**			ON (5.24)

Figure 11. PXRD analysis of the standard screening array, form assignment (top, ON, OP, Y), and crystallinity score (bottom).

well within that range (R = 3.83% O = 3.56%, Y = 3.23%). Additional details are provided in the Supporting Materials section.

It is common to obtain multiple single crystals from a plate that can be analyzed to gain insight into the composition of crystals and establish the absolute stereochemical configuration of our substrates. The corresponding single-crystal data provides valuable information such as to whether the crystals are neat, hydrated, or solvated. The information obtained in this manner helps guide the appropriate follow-up studies at 20−100 mg scale, particularly for cases of compounds with limited supplies in order to maximize the efficiency of material usage.

A final component of integration of high-throughput crystallization screening systems is a transition to the collection of transmission mode PXRD data from the milligram scale crystallization plates. In earlier iterations of this workflow, Raman spectra were collected from quartz 96-well plates; however, there were translational gaps between forms initially observed in 96-well plates with Raman microspectroscopy and forms later identified after scaling up by PXRD analysis. Therefore, it became highly advantageous to directly collect PXRD data from small-scale experiments.

We turned our attention toward bridging this analytical technique gap and developed a standard PXRD protocol. To evaluate this protocol, two highly consistent crystallization systems were selected (isopropanol/water) and (t-amyl-OH/heptane) and each was replicated in a row of a 96-well plate utilizing increasing material loadings to afford 12 replicates of each solvent system at 4 scales (0.5, 1, 2, and 4 mg). In all cases, birefringent crystals were observed via PLM analysis as shown in Figure 7. The samples in each well were subjected to grinding with a magnetic stir bar for 1 h to minimize the preferred orientation followed by slurry transfer and isolation of wet cakes on a PXRD stage filter.

PXRD data collected by this method is illustrated in Figure 8. To better assess the quality of the PXRD patterns, Figure 9 shows the degree of crystallinity[15] whereby crystallinity = crystalline peak area/whole pattern area ×100 for each sample in

https://doi.org/10.1021/acs.oprd.3c00091
Org. Process Res. Dev. 2023, 27, 1437−1444

the array. On the basis of observations from this data set, a crystallinity value below 3.1 corresponds to a PXRD pattern that cannot be visually interpreted. Once the crystallinity reaches >3.1, small peaks can be observed, which sometimes are sufficient to group the PXRD data and compare to other wells. Once the crystallinity score is >4, comparisons can be readily made between wells and forms can be assigned by comparing to literature PXRD patterns, presuming the data is not skewed by the preferred orientation.

Figure 10 illustrates the ability to compare forms obtained from each well of this test study and associate these patterns with known forms in the literature. The ability to assign various forms depends upon the quality of each individual PXRD pattern. As seen in Figure 8 at a loading of at least 2 mg, all PXRD patterns were sufficiently intense (crystallinity score >4) to be able to assign forms in each of the wells. Once the loading drops to 1 mg and 0.5 mg, the PXRD patterns generated by crystallizations from isopropanol/water systems appear to be sufficiently strong to be assigned, whereas materials generated from tert-amyl alcohol/heptane have lower crystallinity and many PXRD patterns could not be assigned.

The ability to collect PXRD data sufficient to estimate the distribution of forms present in the plate is dependent upon a multitude of factors that include crystallinity of the sample, stability of the crystal to isolation, yield of the crystallization, transferability of the sample, and particle size, which impacts the preferred orientation. It was found that particle size reduction by treatment with stir bars prior to transfer prevents large particles from settling outside of the X-ray beam diameter and lessens the degree of preferred orientation of the samples on the PXRD stage filter. Note that an amorphous result by this method can indicate that either the sample is amorphous or the sample did not sufficiently transfer to the PXRD stage filter for the above reasons.

The last step in this study was to apply this analytical technique to our standard array. With a loading of 2 mg ROY/well, crystals of sufficient quality are produced to generate interpretable PXRD data. By PXRD analysis, ROY behaved in a manner similar to other APIs that afford polymorphic distributions upon screening. Figure 11 summarizes form assignments and calculated crystallinity values from one of the six solvent array screens of ROY that is illustrated in Figure 3. Overall, form assignments were made by comparing PXRD patterns to reported simulated PXRD patterns of ROY. In this experiment, form assignments could be made in 41 out of 47 wells that had successfully crystallized. In 6 cases, either insufficient material was isolated or poorly crystalline samples resulted in PXRD patterns that were too weak to assign (crystallinity score 3.0−3.1). The complexity of the form assignments in this example is comparable to typical APIs. The greatest challenges are low signal strength or challenges with a preferred orientation that seem to be mitigated with the stir bar grinding step.

For this example, the crystallization study on ROY with a loading of 2 mg/well successfully analyzed 87% of the successful crystallizations by PXRD, rapidly identified 3 polymorphs, Y, OP, and OR, which would aid in the generation of these forms early in the development cycle, and inform us that there was a complex form landscape for this molecule in a single screening experiment utilizing 200 mg of precious input material.

The software tools enable our scientists to collect, store, process, and share findings from large data intense studies. The key to bridging crystallization data into future data science and machine learning paradigms is the capture of information in a manner that is both human- and machine-readable. An emerging database of crystal images, will facilitate the future development of tools to detect the presence of birefringent crystals, estimate the amount of solids present, characterize morphology, and identify crystals suitable for single-crystal analysis. To that end, the Supporting Information contains examples of standard spreadsheets and metadata capture that were developed to capture experimental details associated with 96-well plate experiments.

The systems described herein are the product of two decades of research and experience. As with any advanced workflow, the starting point should be the simplest iteration, which would consist of a 96-well plate-based crystallizer, a microscope with a long working distance to visualize the samples, and a multichannel pipettor to efficiently move materials. This is the minimal amount of technology required to carry out an early version of this experimental technique. With the generation of initial hundreds of milligrams of purified synthetic organic compounds, the system can rapidly screen for crystalline material to enable the more rapid purification of intermediates and subsequent development of synthetic routes. Success in carrying out initial crystallization studies in these plates provides further incentive to build more advanced systems for the purpose of readily sharing large amounts of data and images for a broad portfolio of organic compounds.

CONCLUSIONS

Using an array of commercially available equipment and robotics, we have described a screening protocol that can reliably and consistently evaluate small-scale crystallizations that are directly analyzed by polarized light microscopy for image acquisition and are thoroughly evaluated by our crystallography team. Using ROY as a surrogate for an unknown API, the crystallization study would have informed us of multiple potential crystallization solvent systems, obtained single-crystal structures, and provided both single-crystal and PXRD evidence that multiple polymorphs exist for this molecule. Solvent combinations that successfully generate crystalline samples, along with images, are captured in a database that is amenable to data science. With compounds of sufficient crystallinity, we have demonstrated the potential to detect PXRD peaks down to 0.5 mg of sample loading with 1 minute of PXRD collection time in transmission mode to afford interpretable PXRD patterns for a 96-well plate experiment. The incorporation of both single-crystal and PXRD analyses provides a thorough form assessment of our screening arrays as we routinely evaluate a portfolio of compounds for our development organization.

ASSOCIATED CONTENT

Supporting Information

The Supporting Information is available free of charge at https://pubs.acs.org/doi/10.1021/acs.oprd.3c00091.

Images and solvent conditions for seven crystallization plates, images of source tubes for single-crystal samples, images of red and yellow crystals mounted on the diffractometer with faces overlaid and drawn with thin black lines and crystal structure images for red, orange and yellow (PDF)

PXRD data files 1 from 96 position loading study (ZIP)

PXRD data files 2 from standard 5-4-3 study (ZIP)

https://doi.org/10.1021/acs.oprd.3c00091
Org. Process Res. Dev. 2023, 27, 1437−1444

AUTHOR INFORMATION

Corresponding Author

Victor W. Rosso − *Department of Chemical Process Technology, Bristol-Myers Squibb, New Brunswick, New Jersey 08903, United States;* orcid.org/0000-0002-1036-4153; Email: Victor.Rosso@BMS.com

Authors

Zhiwei Yin − *Department of Materials Science and Engineering, Bristol-Myers Squibb, Summit, New Jersey 07901, United States*

Heba Abourahma − *Department of Chemistry, The College of New Jersey, Ewing, New Jersey 08628, United States*

Ariel Furman − *Department of Chemical Process Technology, Bristol-Myers Squibb, New Brunswick, New Jersey 08903, United States;* orcid.org/0009-0000-3043-9637

Shasad Sharif − *Department of Materials Science and Engineering, Bristol-Myers Squibb, Summit, New Jersey 07901, United States*

Andrew Werneth − *Department of Materials Science and Engineering, Bristol-Myers Squibb, New Brunswick, New Jersey 08903, United States*

Jason M. Stevens − *Department of Chemical Process Technology, Bristol-Myers Squibb, Summit, New Jersey 07901, United States;* orcid.org/0000-0003-1671-1539

Frederick Roberts − *Department of Chemical Process Technology, Bristol-Myers Squibb, New Brunswick, New Jersey 08903, United States*

Darpandeep Aulakh − *Department of Materials Science and Engineering, Bristol-Myers Squibb, New Brunswick, New Jersey 08903, United States;* Present Address: Veranova, 25 Patton Road, Devens Massachusetts 01434, United States

Roger Sommer − *Department of Materials Science and Engineering, Bristol-Myers Squibb, New Brunswick, New Jersey 08903, United States;* orcid.org/0000-0003-1422-5967

Amy A. Sarjeant − *Department of Materials Science and Engineering, Bristol-Myers Squibb, New Brunswick, New Jersey 08903, United States;* orcid.org/0000-0002-1993-0406

Complete contact information is available at: https://pubs.acs.org/10.1021/acs.oprd.3c00091

Notes

The authors declare no competing financial interest.

ACKNOWLEDGMENTS

The authors would like to acknowledge Michael J. Williams and Joshua Engstrom for their support and review of this manuscript.

ABBREVIATIONS

PXRD, powder X-ray diffraction; ROY, red orange yellow; THF, tetrahydrofuran; MEK, methyl ethyl ketone; MeTHF, 2-methyltetrahydrofuran; DME, 1,2 dimethoxyethane; EtOAc, ethyl acetate; iPrOAc, isopropyl acetate; n-BuOAc, n-butyl acetate; MIBK, methyl isobutyl ketone; MTBE, methyl tert-butyl ether; DCE, 1,2-dichloroethane; CPME, cyclopentyl methyl ether; MeCN, acetonitrile; MeOH, methanol; iPrOH, isopropanol; tert-Amyl-OH, tert-amyl alcohol; CSD, Cambridge Structural Database; Amorph, amorphous; wk, weak

REFERENCES

(1) Tung, H-H.; Paul, E. L.; Midler, M.; McCauley, J. A. *Crystallization of Organic Compounds: An Industrial Perspective*; Wiley, 2009.

(2) Lee, A. Y.; Erdemir, D.; Myerson, A. S. Crystal polymorphism in chemical process development. *Annual review of chemical and biomolecular engineering* **2011**, *2*, 259−280.

(3) Kumar, L.; Amin, A.; Bansal, A. K. An overview of automated systems relevant in pharmaceutical salt screening. *Drug Discovery Today* **2007**, *12*, 1046−1053.

(4) Selekman, J. A.; Qiu, J.; Tran, K.; Stevens, J.; Rosso, V.; Simmons, E.; Xiao, Y.; Janey, J. High-Throughput Automation in Chemical Process Development. *Annu. Rev. Chem. Biomol. Eng.* **2017**, *8*, 525−547.

(5) Morissette, S. L.; Almarsson, O.; Peterson, M. L.; Remenar, J. F.; Read, M. J.; Lemmo, A. V.; Ellis, S.; Cima, M. J.; Gardner, C. R. High-throughput crystallization: polymorphs, salts, co-crystals and solvates of pharmaceutical solids. *Adv. Drug Delivery Rev.* **2004**, *56*, 275−300.

(6) Rodrigues, M.; Lopes, J.; Sarraguça, M. Vibrational Spectroscopy for Cocrystals Screening. A Comparative Study. *Molecules* **2018**, *23*, 3263.

(7) Lowry, S.; Dalrymple, D.; Song, A.; Rosso, V.; Pommier, C.; Venit, J. Integrating a Raman microscope into the workflow of a high-throughput crystallization laboratory. *JALA* **2006**, *11*, 75−84.

(8) Pfund, L. Y.; Matzger, A. J. Towards exhaustive and automated high-throughput screening for crystalline polymorphs. *ACS Combinatorial Science* **2014**, *16*, 309−313.

(9) Sheridan, M. *"Symyx, Merck to develop "Discovery Tools" system"*; ICIS News: June 26, 2001.

(10) Qiu, J.; Patel, A.; Stevens, J. M. High-throughput salt screening of synthetic intermediates: effects of solvents, counterions, and counter-ion solubility. *Org. Process Res. Dev.* **2020**, *24*, 1262−1270.

(11) Qiu, J.; Stevens, J. M. High-throughput classical chiral resolution screening of synthetic intermediates: effects of resolving agents, crystallization solvents, and other factors. *Org. Process Res. Dev.* **2020**, *24*, 1725−1734.

(12) Mitchell, C. A.; Yu, L.; Ward, M. D. Selective Nucleation and Discovery of Organic Polymorphs through Epitaxy with Single Crystal Substrates. *J. Am. Chem. Soc.* **2001**, *123*, 10830−10839.

(13) Singh, A.; Lee, I. S.; Myerson, A. S. Concomitant crystallization of ROY on patterned substrates: Using a high throughput method to improve the chances of crystallization of different polymorphs. *Cryst. Growth Des.* **2009**, *9*, 1182−1185.

(14) Selekman, J. A.; Roberts, D.; Rosso, V.; Qiu, J.; Nolfo, J.; Gao, Q.; Janey, J. Development of a highly automated workflow for investigating polymorphism and assessing risk of forming undesired crystal forms within a crystallization design space. *Org. Process Res. Dev.* **2016**, *20*, 70−75.

(15) Kavesh, S.; Schultz, J. M. Meaning and measurement of crystallinity in polymers: A Review. *Polym. Eng. Sci.* **1969**, *9*, 331−338.